Impact of capillary hysteresis and trapping on vertically integrated models for CO_2 storage

F. Doster[a,b], J.M. Nordbotten[b,a], M.A. Celia[a]

[a] *Dep. of Civil and Environmetal Engineering, Princeton University*
[b] *Dep. of Mathematics, University of Bergen*

Abstract

Vertically integrated models are frequently applied to study subsurface flow related to CO_2 storage scenarios in saline aquifers. In this paper, we study the impact of capillary-pressure hysteresis and CO_2 trapping on the integrated constitutive parameter functions. Our results show that for the initial drainage and a subsequent imbibition, trapping is the dominant contributor to hysteresis in integrated models. We also find that for advective processes like injection and plume migration in a sloped aquifer the correct treatment of the hysteretic nature of the capillary fringe is likely of secondary importance. However, for diffusive/dispersive processes such as a redistribution of the CO_2 plume due to buoyancy and capillary forces, the hysteretic nature of the capillary fringe may significantly impact the final distribution of the fluids and the timescale of the redistribution.

Keywords: Hysteresis, CO_2 Storage, Upscaling, Multiphase Flow, Porous Media, Trapping
76S05 MSC:

1. Introduction

Subsurface two-phase flow processes in geological porous media are relevant to many applications including oil and gas production, CO_2 storage, and ground remediation. These application involve lateral spatial extents on the order of hundreds of meters to tens of kilometers. Furthermore, often only statistical properties of the relevant parameter fields are known. This renders models for the prediction of fluid and contaminant motion computationally demanding.

In many settings, the lateral extent of the relevant domain is large compared to the vertical extent. Consequently, horizontal flow dominates the large-scale dynamics and fluids are often in (or close to) vertical equilibrium [2]. Additionally, for high density contrast between the fluids in a two-fluid system and moderate horizontal driving forces, as in the case of unconfined aquifers and in post-injection plume migration scenarios in CO_2 storage, vertical redistributions occur on relatively short time scales compared to lateral redistributions. In these cases, it is reasonable to assume that the fluids are segregated due to gravity. These approximations permit an integration over the vertical direction, reducing the dimensionality of the problem from 3 to 2 and thereby reducing computational costs significantly. Limits of the vertical equilibrium approximation are investigated in [1, 2]. Consideration of lateral symmetries may eliminate another dimension, and even permit analytical solutions [3, 4, 5, 6].

Integration over the vertical extent generates an upscaled set of equations with new parameter functions that depend on the vertical fluid distributions. The vertical equilibrium assumption provides a framework to reconstruct vertical fluid distributions from the upscaled variables, making explicit determination of the upscaled parameter functions is possible ([7, 8]).

The most common approach in CO_2-storage modeling assumes e.g. a complete segregation of the fluids. In this model – referred to as a sharp interface approximation – the lighter fluid occupies the upper part of the vertical domain and the denser fluid the lower part, and the vertical position of the interface between the two fluids determines the integrated amount of both fluids. The resulting upscaled constitutive functions (relative permeabilities and capillary pressure) are linear with respect to the integrated (upscaled) saturations, permitting attractive analytic treatment (see e.g. [3, 4, 5, 6, 9] for examples). Increasing the level of detail in the reconstruction of the fluid distribution requires choices about additional phenomena to be taken into account. Recently, the inclusion of an explicit capillary transition zone was explored in the context of CO_2 storage [10, 11, 12]. Therein, the balance of capillary and gravitational forces determined the vertical fluid structure. However, in those and later studies, process and path dependence (hysteresis) of the fine-scale constitutive functions has been largely ignored.

In this contribution, we explore the impact of hysteretic fine-scale constitutive functions on the upscaled constitutive functions that appear in the application of CO_2 storage. The article is structured as follows. In the next section we give a brief review of the fine-scale equations including a trapping

model for CO_2 and a model for capillary pressure which captures hysteresis. The subsequent section presents the applied upscaling procedure – vertical integration – and limiting cases of it. In the results section we discuss the implications of fine-scale trapping and process-dependent capillary pressure on the upscaled constitutive functions. The paper closes with concluding remarks.

2. Model equations for CO_2 storage

In this section, we give a brief review of the established equations for porous media flow, as they apply to the problem of CO_2 storage. For simplicity of exposition we focus on the phenomena related to hysteresis in the constitutive relationships, rather than on full generality of geometry and heterogeneity. For more general derivations in this respect we refer to the literature [7, 8].

Consider two immiscible and incompressible fluids and a rigid porous medium under isothermal conditions. The fluids are distinguishable by their wetting properties and we denote one fluid as the wetting fluid w and the other as the non-wetting fluid n. The two fluids have different densities ρ where we assume by convention that $\rho_w > \rho_n$ (the opposite case is analogous). The connected pore space $V_\phi = \phi V$, with porosity ϕ and sample volume V, is filled with the two fluids. The fluid volumes are expressed in terms of saturations $s_\alpha = V_\alpha / V_\phi$ with $\alpha \in \{w, n\}$ denoting the corresponding fluid. By this definition

$$s_w + s_n = 1 \tag{1}$$

holds true. For this incompressible case mass, and volume conservation are equivalent and we obtain

$$\frac{\partial \phi s_\alpha}{\partial t} + \nabla \cdot \mathbf{u}_\alpha = 0, \tag{2}$$

when sources are absent. The fluid flux is denoted by $\mathbf{u}_\alpha$. We assume that the fluid flow is governed by the extended Darcy law

$$\mathbf{u}_\alpha = -\lambda_\alpha k \left(\nabla p_\alpha - \rho_\alpha \mathbf{g} \right) \tag{3}$$

with a scalar mobility λ_α of phase α, a scalar permeability k, the fluid pressure p_α, and the gravity acceleration vector $\mathbf{g}$. The scalar mobility relates to

the relative permeability through the viscosity μ_α as $k_{r\alpha} = \lambda_\alpha \mu_\alpha$. The phase pressures are related by the capillary pressure function

$$p_{\text{cap}} = p_n - p_w. \tag{4}$$

We assume that the capillary pressure and the relative permeability functions are algebraic functions and depend only on saturation and the saturation history. An explicit spatial dependency is neglected for the sake of clarity. The contribution of other variables and effects such as e.g. specific interfacial area [13], connectivity of the fluids [14], dynamic effects [15] or apparent surface tensions [16] is active ongoing research but not considered here. The Equations (1)-(4) form a set of 10 equations for 10 unknowns in three dimensions. They form a closed and solvable system, provided that explicit parametrizations for p_{cap} and $k_{r\alpha}$ and proper initial and boundary conditions are given.

While the results and methodology of this paper are applicable for any constitutive functions, we will for concreteness specify a typical choice of such models here.

2.1. Capillary pressure

We take a van Genuchten parametrization for the capillary-pressure-saturation relation, [17]

$$p^\chi_{\text{cap}}(s_w) = p^\chi_e \left(s_w^{-\frac{1}{m}} - 1 \right)^{\frac{1}{n}} \tag{5}$$

with the characteristic pressure p^χ_e and exponents n, m. The superscript $\chi \in \{d, i\}$ indicates drainage (d) and imbibition (i) values. Our approach and results can be extended to any other parameterization, including the popular Brooks-Corey functions.

Correspondingly, we denote the inverse capillary-pressure function as s_{cap}, which in the van Genuchten parameterization reads

$$s^\chi_{\text{cap}}(p_{\text{cap}}) = \left[(p_{\text{cap}}/p^\chi_e)^n + 1 \right]^{-m}. \tag{6}$$

Here, it is implied that the inverse capillary pressure function always refers to the wetting phase.

2.2. Relative permeabilities

We take a Brooks-Corey parameterization [18] of relative permeabilities,

$$k_{rw}(s_w) = s_w^4, \tag{7}$$

$$k_{rn}(s_w) = k_{rn}^{max} \left(1 - s_w\right)^2 \left(1 - {s_w}^2\right), \tag{8}$$

where we use an effective brine saturation that accounts for the irreducible brine saturation, and k_{rn}^{max} is a parameter added to account for the reduced maximal permeability at irreducible brine saturation with respect to the non-wetting phase which is often observed in CO_2 storage [19].

2.3. Hysteresis model for capillary pressure

The capillary pressure curve between the bounding capillary curves is commonly obtained by scaling the section of the corresponding main drainage / imbibition curve which is covering the same pressure difference onto the corresponding saturation interval [20, 21]. In this setting, the corresponding interval is bounded by an upper and lower turning saturation (usually the two last turning points - see Figure 1). Mathematically, this can be expressed in terms of the inverse capillary pressure saturation relationship

$$s_{\mathrm{cap}}(p_{\mathrm{cap}}) = \frac{s^i_{\mathrm{cap}}(p_{\mathrm{cap}}) - s^i_{\mathrm{cap}}(\underline{p}_{\mathrm{cap}})}{s^i_{\mathrm{cap}}(\bar{p}_{\mathrm{cap}}) - s^i_{\mathrm{cap}}(\underline{p}_{\mathrm{cap}})} \left(\bar{s}_w - \underline{s}_w\right) - \bar{s}_w \tag{9}$$

Here, underscore and overscore refer to the lower and upper turning point, respectively, as applied to saturation and pressure. This expression is written for an increasing s_w from the last turning point. In the reverse case, the functions s^d_{cap} are used instead of s^i_{cap}. If the saturation leaves the interval $[\underline{s}_w, \bar{s}_w]$ the next confining turning points are taken. Note, that at turning points the capillary-pressure-saturation relation is not differentiable but remains continuous for the van Genuchten parametrization. For a Brooks-Corey parametrization, scanning curves are discontinuous for saturations larger than a critical saturation due to the finite capillary pressure.

2.4. Trapping model

The hysteresis model for the capillary pressure as given in the preceding section, leaves the residual saturation independent of process history. However, this does not hold true in general, and Land [22] observed that the difference of the reciprocals between the maximum non-wetting saturation

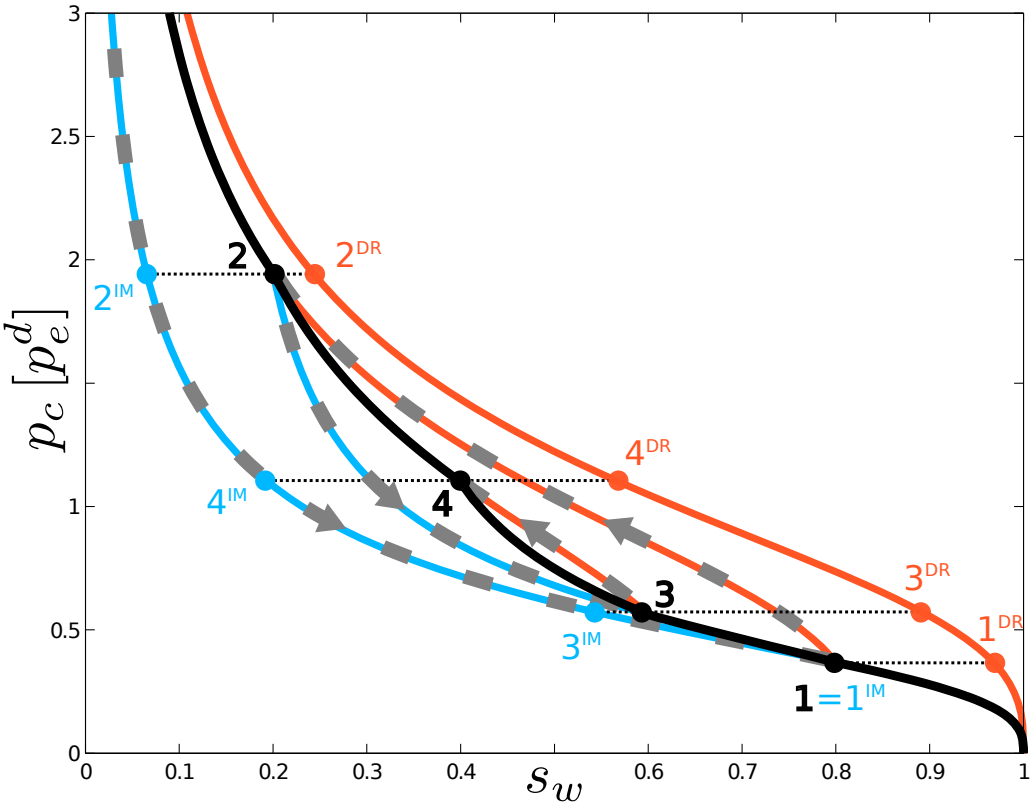

Figure 1: Illustration of the scaling concept for hysteretic capillary pressure. The blue lines show imbibition curves and the red lines drainage curves. A possible process path is shown by grey dashed curves with arrows indicating the process direction. Turning points are marked by black dots and their corresponding capillary pressure values on the bounding drainage curve by red dots and on the bounding imbibition curve by blue dots. The full hysteretic capillary-pressure-saturation relationship for the process history is depicted by a solid black line.

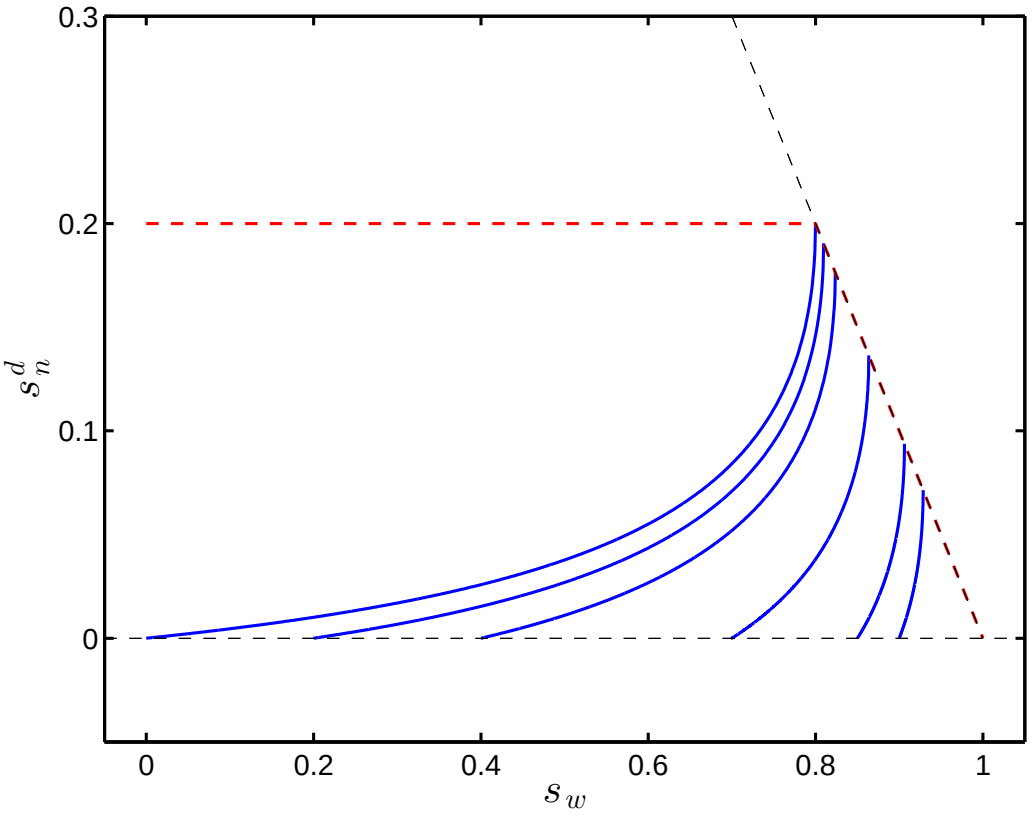

Figure 2: Illustration of the Land trapping model for for $s_n^{\text{res}} = 0.2$ and $s_n^{\max} = \{1, 0.8, 0.6, 0.3, 0.15, 0.1\}$ (blue lines) and the irreducible gas saturation model (red dashed curve).

$s_n^{\max}$ and the non-wetting residual saturation s_{nr} is approximately constant for a given system. Hence, the measurement of one pair, e.g. the extreme values $s_n^{\max} = 1$ and the residual saturation of the primary imbibition loop s_n^{res}, suffices to determine the relationship

$$s_{nr}(s_n^{\max}) = \frac{s_n^{\max}}{1 + (1/s_n^{\text{res}} - 1)s_n^{\max}}. \tag{10}$$

In other words, the residual saturation of the actual process is history-dependent, and determined based on both the residual saturation of the primary loop as well as the maximum attained saturation of the process.

To obtain a full model, Land further introduced the notion of the non-wetting phase being partitioned in connected and disconnected fractions, denoted s_n^c and s_n^d, respectively. The connected fraction is considered mobile, while the disconnected is considered immobile. Hence, only the connected fraction will be of importance for relative permeability.

To close this model, Land postulated that Equation (10) also holds for the connected non-wetting phase,

$$s_{nr}(s_n^c) = \frac{s_n^c}{1 + (1/s_n^{\text{res}} - 1)s_n^c}; \tag{11}$$

i.e. for a given connected non-wetting phase saturation the same amount gets trapped after a completed imbibition independent of how much disconnected non-wetting fluid is currently present. Furthermore, he assumed that the non-wetting fluid is completely connected at the maximum non-wetting saturation $s_n^{\max}$. Hence, the disconnected non-wetting saturation is determined by $s_n^d(s_n^c; s_n^{\max}) = s_{nr}(s_n^{\max}) - s_{nr}(s_n^c)$. Using the relationship that the disconnected non-wetting saturation is simply the difference between the non-wetting saturation and the connected fraction, e.g. $s_n^d = s_n - s_n^c$, we can then obtain

$$\begin{aligned} s_n^d(s_n; s_n^{\max}) = \frac{1}{2}\Bigg[& (s_n + s_{nr}(s_n^{\max})) \\ & - \sqrt{\left(s_n - s_{nr}(s_n^{\max})\right)^2 + \frac{4}{1/s_n^{\text{res}} - 1}\left(s_n - s_{nr}\left(s_n^{\max}\right)\right)}\Bigg]. \end{aligned} \tag{12}$$

This model has been derived for a system of water and hydro-carbon gas,

but it is proposed to hold also for other fluid pairs, in our context supercritical CO_2 and water. Even though the model is constructed for imbibition processes, Land [22] suggests that the difference between drainage and imbibition is expected to be small and Equation (12) holds for drainage processes as well. Figure 2 illustrates $s_n^d(1 - s_w; s_n^{\max})$ for $s_n^{\text{res}} = 0.2$ and $s_n^{\max} = \{1, 0.8, 0.6, 0.3, 0.15, 0.1\}$ with solid blue lines.

The trapped or disconnected non-wetting phase is incorporated into the capillary-pressure-saturation concept by assuming that the disconnected nonwetting phase is completely embedded in the wetting phase. From a geometric perspective, the trapped nonwetting phase then appears as a part of the overall volume occupied by the wetting phase. We therefore denote the sum of the wetting phase and the trapped nonwetting phase as the apparent saturation [21], defined as

$$\sigma_w = s_w + s_n^d. \tag{13}$$

It follows, that the apparent non-wetting saturation can be identified as the connected component of the non-wetting phase, $\sigma_n = s_n^c$.

These apparent saturations are now utilized in both the non-wetting relative permeability, as well as in the capillary pressure functions, of the preceding sections but not in the wetting relative permeability. The physical idea for this choice is that the disconnected non-wetting phase that is surrounded by the wetting phase increases the apparent volume of the wetting fluid. The connected non-wetting phase is distributed identically and the apparent saturation yields the appropriate relative permeability. For the wetting-phase relative permeability, however, the disconnected non-wetting phase must not be taken into account because it does not contribute to the flow of the wetting phase.

We close the description of trapping models by pointing out a simple special case, which is commonly referred to as irreducible gas saturation. In this model, any non-wetting saturation below s_n^{res} is considered disconnected and immobile. Thus

$$s_{nr} = \min(s_n^{\max}, s_n^{\text{res}}) \tag{14}$$

This simplified trapping model has been used by several authors in the context of CO_2 storage [23, 24, 25, 11], and we will include it in the discussions of later sections. It is illustrated in Figure 2 by dashed red lines.

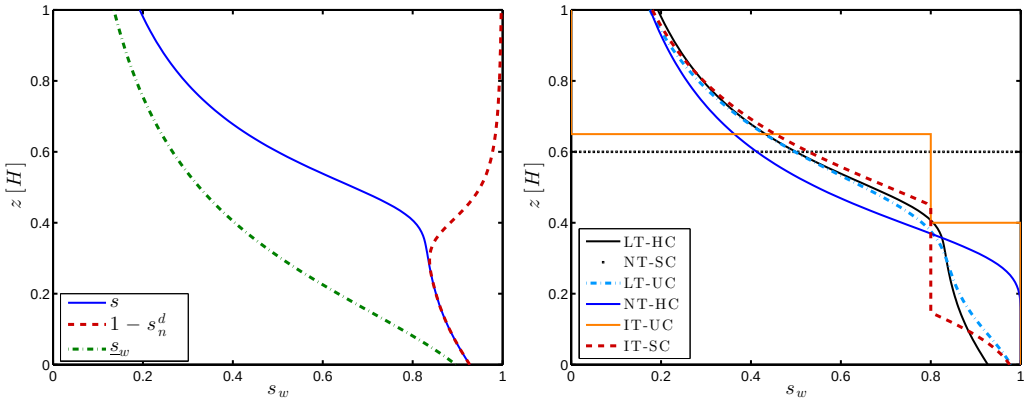

Figure 3: Illustration of vertical wetting saturation s_w for a secondary imbibition. Figure (a) shows saturation distributions for the full model, the turning profile and the disconnected non-wetting saturation plotted as $1 - s_n^d$. Figure (b) shows the wetting saturation s_w for models with varying complexity. The abbreviations for the models are given in Table 1.

3. Vertically integrated equations

In subsurface flow processes, and in particular those related to CO_2 storage, the lateral extent of interest is often substantially larger (kilometers to tens of kilometers) than the vertical extent (meters to tens of meters). Further, vertical fluid redistribution often happens on time-scales much shorter than horizontal fluid redistributions, and the vertical fluid distribution may be considered to be in hydrostatic equilibrium. A more detailed estimation and description of involved time-scales is given in [8, 10]. For the sake of clarity we assume that in the vertical direction the domain - referred to as the reservoir - is bounded in the vertical by impermeable layers, that the bounds are perpendicular to the gravity vector and that the distance H between them is constant in the whole reservoir. We choose to express terms in a cartesian coordinate system where the z-axis is aligned opposite to gravity. Further we assume for simplicity that permeability k and porosity ϕ do not vary along the vertical direction.

The aim of the vertical integration is to obtain equations for the horizontal coordinates with variables representative of quantities over the entire vertical extent of the reservoir. We refer to the vertical domain as the fine scale and to the horizontal extent as the coarse scale. Fine-scale quantities are denoted by lower-case letter and coarse-scale quantities by upper-case letters. Equation

(3) implies that the pressure gradient in each phase compensates buoyancy in the vertical hydrostatic equilibrium ($u_{\alpha z} = 0$). Hence, the pressure at any vertical position can be obtained by integrating from the value at a reference position. We normalize the z-axis in terms of the reservoir height H with $z = 0$ at the bottom and $z = 1$ at the top of the reservoir and choose the top as reference position

$$P_\alpha = p_\alpha(z = 1). \tag{15}$$

The reconstructed pressure then is

$$p_\alpha(z) = P_\alpha + \rho_\alpha g H(1 - z). \tag{16}$$

The other coarse-scale quantities are introduced by integrating or averaging the fine-scale quantities. We assume a homogeneous system with isothermal and incompressible fluids. We have normalized the vertical axis to the reservoir height and write the equations in dimensionless form. In the incompressible, homogeneous case, the coarse-scale equivalents of porosity $\Phi = H\phi$, density $R_\alpha = \rho_\alpha$, viscosity $M_\alpha = \mu_\alpha$ and permeability $K = Hk$ all equal their fine-scale counterparts.

Following [8], the coarse solution variables and the constitutive forms are related to the fine scale through

$$S_\alpha = \frac{1}{\Phi} \int_0^1 \phi s_\alpha \mathrm{d}z, \tag{17}$$

$$\mathbf{U}_\alpha = \int_0^1 \mathbf{u}_{\alpha||} \mathrm{d}z, \tag{18}$$

$$K_{r\alpha} = \frac{1}{K} \int_0^1 k k_{r\alpha}(s_\alpha(z)) \mathrm{d}z. \tag{19}$$

We emphasize that simplifying assumptions have been applied extensively and refer to [8, 10] for a less restrictive formulation. The subscript $||$ denotes the horizontal components and $\mathbf{U}_\alpha$ is a two-dimensional vector. With these definitions the integral of Equation (2) over the vertical extent is given by

$$\frac{\partial \Phi S_\alpha}{\partial t} + \nabla_{||} \cdot \mathbf{U}_\alpha = 0 \tag{20}$$

with the coarse-scale Darcy law

$$\mathbf{U}_\alpha = -K\Lambda_\alpha \left(\nabla_{||} P_\alpha - R_\alpha \mathbf{G}\right) \tag{21}$$

and a two-dimensional horizontal operator $\nabla_{||}$. Like on the fine scale, the coarse-scale relative permeability and mobility are related through the viscosity $K_{r\alpha} = \Lambda_\alpha M_\alpha$ and also the pore volume is conserved

$$S_w + S_n = 1. \tag{22}$$

The coarse-scale capillary pressure function is similarly defined as

$$P_{\text{cap}}(\cdot) = P_n - P_w, \tag{23}$$

where we use the notation $(\cdot)$ to highlight that the arguments of the capillary pressure function are yet to be determined.

As seen from Equation (19), the vertical fine-scale saturation distributions $s_w(z; x, y)$ are required to obtain coarse-scale effective parameter functions. Therefore, a reconstruction procedure for s_w has to be provided for a pure coarse-scale model. The assumption of hydrostatic fluid distribution allows for such a reconstruction. From Equation (16) we obtain that the fine-scale capillary pressure has to compensate for buoyancy due to the density difference. From this the fine-scale capillary pressure can be constructed and related to the coarse-scale capillary pressure

$$p_{\text{cap}} = P_{\text{cap}} - (\rho_w - \rho_n) g H (1 - z). \tag{24}$$

A well-defined $p_{\text{cap}}(s_w)$ relationship provides invertible $p_{\text{cap}} - s_w$ mappings from which we can reconstruct the vertical saturation distribution for a given P_{cap} and obtain a $P_{\text{cap}} - S_w$ relationship with Equation (17). We can then use this relationship to obtain the fine-scale saturation distribution $s_w(z; x, y)$ for a given coarse-scale saturation S_w and hence are able to express the coarse-scale relative permeabilities $K_{r\alpha}$ in terms of coarse-scale saturations as well. Special cases where the coarse-scale constitutive functions can be derived explicitly have been studied previously [26, 11]. For convenience, we provide an outline of the calculations necessary for a secondary imbibition in the appendix. The consequences of this reconstruction in the case where the p_{cap} relationship entering Equation (4) is fully hysteretic, as described in the previous section, forms the topic of this paper.

3.1. Simplifications and limiting cases

Several limiting cases, or simplifications of the full equilibrium upscaling given in the previous section have been reported. We will briefly summarize and illustrate these models here, as they form the basis for the comparisons presented in the results section. For overviews of these special cases, see e.g. [2, 7, 8]. Note, that the equilibrium upscaling itself is an approximation. However, in many cases it is a good one. In this manuscript we investigate the importance of hysteresis and trapping in the vertical equilibrium approximations for these cases. We structure the models according to how they treat trapping of the non-wetting phase and the capillary fringe. Both phenomena are considered with two levels of simplifications. Table 1 provides an overview and abbreviations for each model.

To fix ideas, we first give the natural dimensionless group for the coarse model, which represents the balance of gravitational and capillary forces, the latter represented by the characteristic pressure for drainage

$$B \equiv \frac{(\rho_w - \rho_n)gH}{p_e^d}. \tag{25}$$

We will refer to this dimensionless group as the Bond number for the system.

For reservoirs with a large Bond number B, the gravitational forces dominate, and the effect of capillary forces can be neglected. Then, the fluids segregate strictly according to density, and the fluid distribution can be described solely based on the segregation height. This height is commonly referred to as an interface (in the coarse sense), and the resulting model is referred to as a sharp interface model (in the following abbreviated by SC, [27, 28]). If the capillary forces impact the fluid distribution, a common approach is to neglect the hysteretic nature of the capillary pressure – saturation relationship and use a representative unique relationship (in the following abbreviated by UC, [11, 12]) as an approximation. We will dis-

Phenomenon	Trapping	Capillary fringe
Model	No (NT)	Sharp interface (SC)
	Irreducible gas (IT)	Unique (UC)
	Land (LT)	Hysteretic (HC)

Table 1: Overview of discussed trapping and capillary fringe models.

cuss the legitimacy of this approach in the results section. Further, the full hysteretic capillary pressure model will be denoted by HC.

With respect to trapping, two simplifications of the full Land trapping model (LT) are commonly used. The simplest approach considers residual trapping as a higher-order process and ignores it completely (we abbreviate it by NT). For large Bond numbers, the capillary transition zone is negligible. This means that at each vertical position the porous medium is either saturated by brine or CO_2. The Land trapping model then collapses to a single irreducible saturation at each position that has been reimbibed. The model is often also applied to systems that include the capillary fringe. It requires a slight modification for domains that have never been drained to the irreducible CO_2 saturation. The explicit form of this modification is usually of minor importance because it only applies to a small region. Here, we assume that all CO_2 gets trapped once the medium is reimbibed and the CO_2-saturation has never been drained to the irreducible CO_2-saturation. We refer to the model as irreducible gas model (IT).

The combination of the three trapping models and the three capillary fringe models permit nine combinations. We illustrate six of these in Figures 3. Both figures show the fluid saturation (x-axis) in a vertical section. The section has initially been drained by CO_2, which is the non-wetting, lighter fluid, from the top down to a coarse (integrated) saturation of $S_w = 0.4$ (green dash-dotted line in Figure 3a), after which brine, which is the wetting, denser fluid re-imbibes from below to a coarse saturation of $S_w = 0.6$. The parameters used are $B = 2$, $n = 4$, $m = 0.5$, $p_e^i/p_e^d = 1/2$ and $s_n^{\text{res}} = 0.2$. Figure 3a shows the saturation distributions for the full model LT-HC. The solid blue line shows the final wetting saturation. The area to the right of this curve is appropriately interpreted as the non-wetting saturation. Additionally, the disconnected non-wetting phase, plotted as $1 - s_n^d$, is shown by the red dashed line. We consider this model as the reference model in this paper, to which the simpler models are compared.

Figure 3b illustrates the same case as Figure 3a, but includes the simplified models and only shows the final wetting-phase saturation. The models are organized in three groups indicated by different color schemes. For reference the extreme models, LT-HC and NT-SC, are depicted black. The models IT-UC and IT-SC have been used in the literature and are depicted as reddish curves. The bluish curves represent partial simplifications of the full model: LT-UC ignores the hysteretic nature of the capillary fringe and NT-HC trapping of the non-wetting phase. We note that in terms of the mod-

els presented, trapping plays a dominant role compared to capillary pressure hysteresis. Indeed, ignoring the hysteretic nature of capillary pressure (light blue dash dotted line) has apparently negligible impact while ignoring trapping markedly changes the fluid distribution (solid dark blue curve). The model with a unique capillary fringe and irreducible gas trapping IT-UC represented by the red dashed curve does a good job while the sharp interface models are significantly off since $B = 2$ can not be considered large. Note, that accounting for trapping (IT-SC, orange solid curve) improves the distribution significantly compared to the pure sharp interface model (NT-SC, black dotted curve). We recall that the vertical fluid distributions in Figure 3 form the basis from which the coarse-scale constitutive functions are calculated in the next section.

4. Results and discussion

In this section, we apply the previously discussed reconstruction methods to study the impact of trapping and hysteretic capillary pressure functions on vertically integrated constitutive functions.

We consider the results in two parts. First, we consider the primary drainage and secondary imbibition loops, which are of immediate importance for CO_2 storage. In this part, we will see that trapping is the most important mechanism, and that simplified models retaining this aspect are in reasonable qualitative agreement with the full model. However, constitutive functions obtained by simplified models may be nearly a factor 2 in error in quantitive terms, even for the primary process.

Secondly, we consider the tertiary drainage and quaternary imbibition, which are needed for more non-trivial exploitation of a storage resource, such as either advanced injection strategies, re-opening of a closed storage site, or remediation strategies for aborted storage locations. In these cases, the simplified models are not adequate, as they do not capture the tertiary and quaternary effects, and we highlight the qualitative aspects of the resulting coarse-scale models.

Throughout we have chosen a Bond number $B = 2$, as an example of a system wherein capillary and gravitational forces are of competing importance. At high Bond numbers, the results would tend toward the sharp interface limit, while at low Bond numbers, there is no difference between the scales, and the fine-scale constitutive functions would be recovered. Further we use the parameters $n = 4$, $m = 0.5$, $p_e^i/p_e^d = 1/2$, $\mu_w/\mu_n = 5$ and

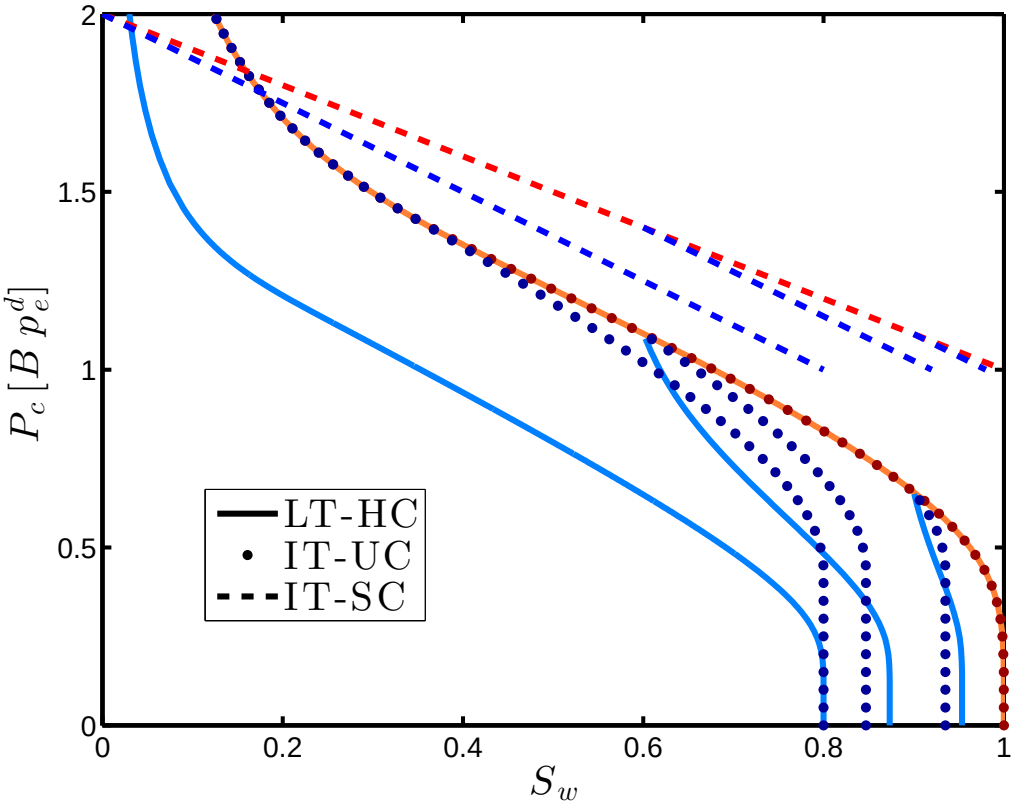

Figure 4: Representative coarse-scale capillary pressure functions for primary drainage (reddish curves) and examples for secondary imbibitions (bluish curves) that start from the integrated saturations $S_w \in \{0,\ 0.6,\ 0.9\}$. Curves with the same line style represent the same model but different processes. The abbreviations for the models are given in Table 1. Note that the absolute value for the IT-SC model is arbitrary, and the curves have been placed above the other curves for clarity.

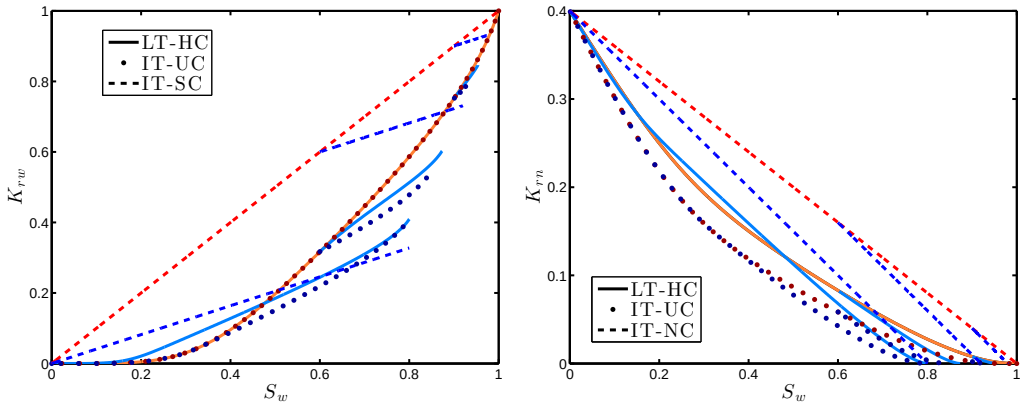

Figure 5: Representative coarse-scale (a) wetting-phase relative permeability and (b) nonwetting-phase relative permeability for primary drainage (reddish curves) and examples for secondary imbibitions (bluish curves) that start from the integrated saturations $S_w \in \{0,\ 0.6,\ 0.9\}$. Curves with the same line style represent the same model but different processes. The abbreviations for the models are given in Table 1.

$s_n^{\text{res}} = 0.2$. Even though a thorough quantitative assessments requires taking into account the particular shape of the constitutive functions, we find that Bond numbers $B > 20$ may be considered large and $B < 0.2$ small. For a more comprehensive study see [12, 26].

4.1. Primary drainage and secondary imbibition

Injection of CO_2 into a brine saturated reservoir as a non-wetting phase leads to a primary drainage process. As injection comes to a halt, and brine re-imbibes into certain regions during the migration period, secondary imbibition processes also take place in the reservoir. These two processes and their representation in the upscaled parameter functions form the focus of this section.

We evaluate the impact of capillary pressure hysteresis and a realistic trapping model on macroscopic fluid migration. Therefore, we compare the full model of hysteresis and trapping (LT-HC) to the two most commonly applied simplified models - the sharp interface capillary fringe with irreducible gas trapping (IT-SC) and the non-hysteretic capillary fringe with irreducible gas trapping (IT-UC). Example vertical saturation distributions for these three models are shown in Figure 3b as a black solid curve (LT-HC), a red dashed curve (IT-HC) and a solid orange curve (IT-SC). We refrain from

illustrating the other model combinations to avoid over-crowding the figures but discuss their qualitative behavior in the text.

Figures 4 and 5 show the calculated coarse-scale capillary pressure and relative permeability functions for primary drainage and example secondary imbibition processes that start from the integrated saturations $S_w \in \{0,\ 0.6,\ 0.9\}$. Figure 4 shows the coarse-scale capillary pressure functions, normalized by the gravitational forces (expressed as the product of the Bond number and entry pressure). Note that for the sharp interface curves, the absolute value of the curves is somewhat arbitrary, and they have been placed above the other curves for clarity. Figures 5a and 5b show the calculated coarse-scale relative permeabilities of the brine and CO_2 phases, respectively. Reddish curves represent the results for the primary drainage process while bluish curves represent secondary imbibition processes.

For all coarse capillary-pressure and wetting-phase relative-permeability functions, the IT-UC model captures the functional form during primary drainage exactly. This is not surprising because we have parametrized the unique capillary pressure relationship with the drainage entry pressure, and disconnected non-wetting phase is not produced during drainage according to LT. The non-wetting relative permeability curves differ, however, because the IT model assumes that the irreducible saturation of non-wetting fluid is immobile even during primary drainage. Hence, the relative permeability is smaller than for the full model. The sharp-interface model IT-SC leads to a linear relationship between the end-point values.

During secondary imbibition, the picture becomes more complicated. First, we note that the full model of fine-scale capillary forces (LT-HC) leads to non-trivial behavior in all coarse constitutive functions. Indeed, the coarse capillary pressure functions displays scaling curves with inflection points separate from either bounding curve. The difference between imbibition and drainage capillary pressure permits stable saturation discontinuities even in homogeneous media. This has been observed recently in [29]. It is not possible to map this phenomenon with UC. In typical examples [28, 30] this phenomenon reduces the spreading after injection has ceased. Further, the coarse-scale relative permeabilities of both phases obtained by the full model lead to crossing curves, even for the main loops. This phenomenon is emergent in the coarse model, and does not exist in the fine model, wherein positive trapping leads to relative permeabilities during secondary imbibition that are strictly below the relative permeabilities of primary drainage. This feature is not captured by either of the simplified models (IT-UC, IT-SC).

Nevertheless, an important metric such as trapped coarse-scale saturation (inferred from the end-points of the coarse capillary pressure and non-wetting relative permeability curves) is reasonably well captured by all models, despite their apparent differences at moderate saturations.

Figure 3b shows profiles for three more model combinations – these have not been represented in Figures 4 and 5 for clarity. The NT-SC model results are identical to the primary drainage curves for IT-SC. The capillary pressure curves of the NT-HC resemble the ones of LT-HC. However, all imbibition curves reach complete saturation again and the difference between the drainage and imbibition bounding curves is smaller. The relative permeability curves are, however, completely different and imbibition relative permeabilities are larger (see [26] for a discussion). The curves of the LT-UC model are similar to the IT-UC model except for the non-wetting phase relative permeabilities. These are close to the full model but do not include the crossing. We also note that the upscaled parameter functions for primary drainage and secondary imbibition are not very sensitive to the particular parametrization of the fine-scale capillary pressure and relative permeability functions.

4.2. Tertiary drainage and quaternary imbibition

From the perspective of storage security, it may be beneficial to actively manage the storage reservoir, varying injection of CO_2 and brine at different points in either space or time [1]. Together with the occurrence of non-trivial flow patterns, there arises a need to consider more than the primary and secondary drainage and imbibition curves.

The general upscaling framework described in section 3 allows for arbitrary high-order saturation histories, however we will limit the discussion to the tertiary and quaternary curves. As seen in the previous sub-section, the process of fine-scale trapping represents the first-order mechanism that introduces hysteretic constitutive functions on the coarse scale. For the tertiary and quaternary processes, this is no longer the case; we see from the Land trapping model (and Figure 2) that trapping only depends on extreme saturations while capillary pressure hysteresis depends on the whole process history. The simplified models explored in the previous sub-section do not capture the hysteresis associated with higher-order processes, and we will in this section only focus on the implications of the full hysteresis model.

Typical constitutive functions associated with a sample of tertiary and quaternary loops are shown in Figures 6 and 7 . Figure 6 shows the typical

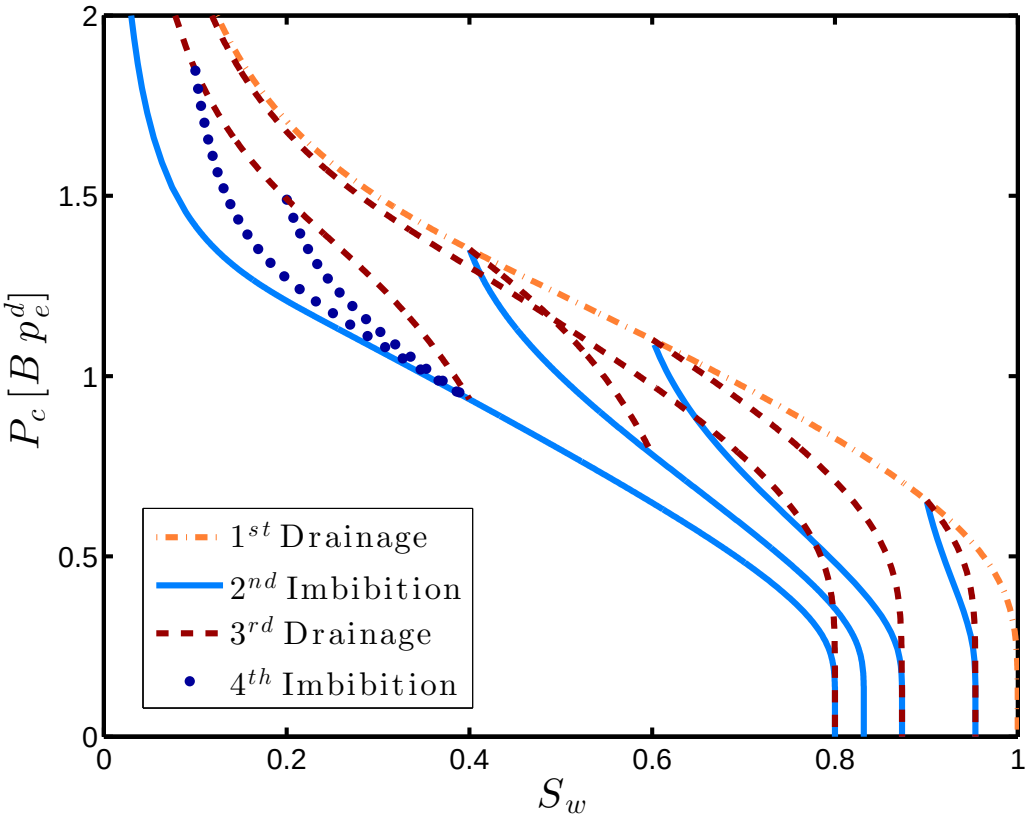

Figure 6: Representative coarse capillary pressure constitutive functions associated with tertiary drainage and quaternary imbibition, shown as dark red dashed and dotted dark blue curves, respectively. For reference, the main features of Figure 4 are repeated in this Figures by orange dash-dotted and solid light blue curves.

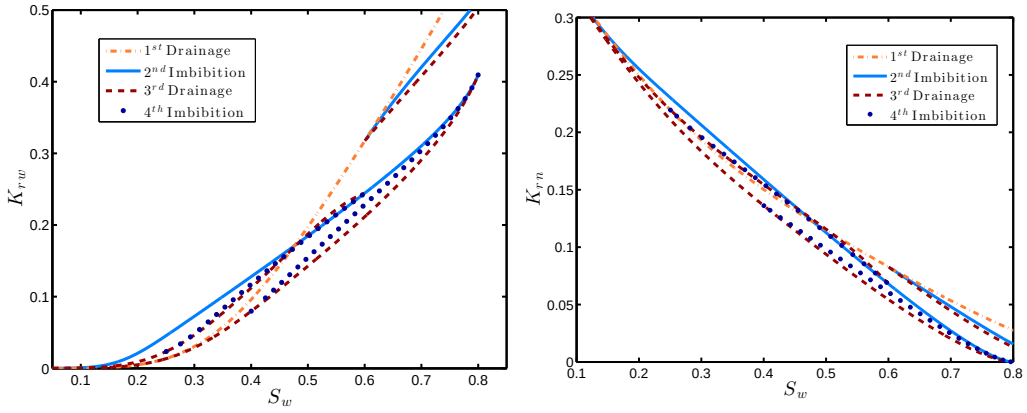

Figure 7: Representative coarse relative permeabilities for the (a) wetting and the (b) non-wetting phase associated with tertiary drainage and quaternary imbibition, shown as dark red dashed and dotted dark blue curves, respectively. For reference, the main features of Figure 5 are repeated in this Figures by orange dash-dotted and solid light blue curves. Note, that the figures do not display the whole range of the functions to emphasize distinctive features.

scanning curves for the coarse capillary pressure function, resulting from the upscaling of the full model (LT-HC). Note that the characteristic behavior of scanning curves departing the primary and secondary curves at angles carries over from the fine-scale, and implies that the derivative of the capillary pressure function is undefined at turning saturations. Figures 7a and 7b again show the coarse relative permeability curves. We note that the tertiary and quaternary processes do not follow the paths of the primary and secondary curves, and indeed may lead to values of coarse relative permeabilities that are outside the range of values from the primary and secondary processes.

To better appreciate the subtleties associated with the higher-order processes, we consider three derived quantities of importance for fluid flow. For flow regimes that can be approximated as incompressible, it is usual to extract characteristic information of the flow system from the fractional flow formulation [31]. Critical in this formulation are the simple fractional flow function, the fractional flow function for gravity driven plume migration in a dipped reservoir, and the function for multi-phase dispersion due to capillary

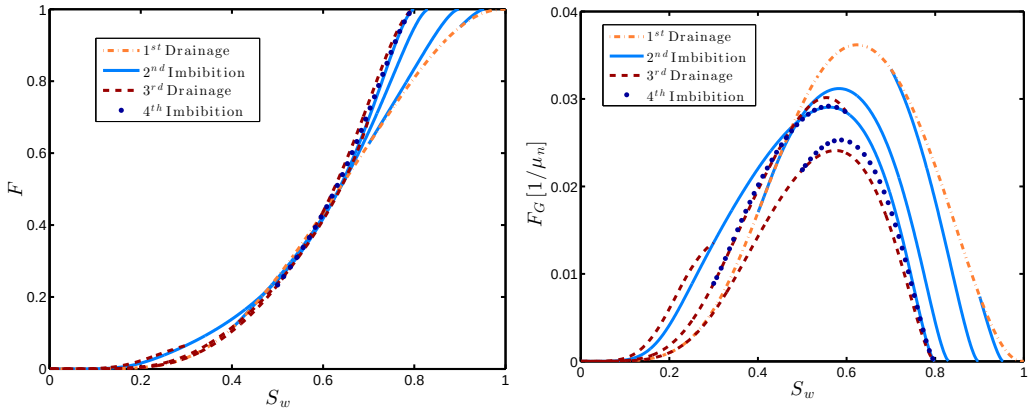

Figure 8: Fractional flow (a) and fractional flow for gravity-driven plume-migration (b) for higher-order drainage and imbibition processes.

forces. These are denoted by F, F_G and D respectively and read as

$$F = \frac{\Lambda_w}{\Lambda_w + \Lambda_n}, \tag{26}$$

$$F_G = \frac{\Lambda_w \Lambda_n}{\Lambda_w + \Lambda_n}, \tag{27}$$

$$D = K \frac{\Lambda_w \Lambda_n}{\Lambda_w + \Lambda_n} \frac{\mathrm{d}P^{\mathrm{c}}}{\mathrm{d}S_w}. \tag{28}$$

We provide these derived functions in Figure 8.

The functions in Figures 8 and 9 allow us to make some general inferences regarding the expected impact of hysteresis, not only on the coarse constitutive functions, but also on the resulting flow patterns. Indeed, the three parameter functions paint quite separate pictures. Firstly, all the imbibition and drainage loops lead to fractional flow functions that are within a small spread of the fractional flow functions of primary drainage and secondary imbibition. Thus, for strongly advective systems, where the fractional flow is of primary importance, i.e. the injection period of CO_2, the detailed treatment of higher-order drainage and hysteresis patterns may be unnecessary.

Secondly, the imbibition and drainage loops are amplified in the fractional flow function for gravity-driven plume migration. The difference between first drainage and secondary imbibition is much larger than in higher-order pro-

cesses. Hence, neglecting higher-order patterns induced by a fully hysteretic capillary pressure function can be considered a good approximation as long as trapping is accounted for. However, one should keep in mind that buoyancy driven imbibition fronts are faster and drainage fronts are slower when hysteresis is taken into account. This changes explicit numbers slightly but does not change the qualitative statements of plume migration in [28, 32, 30].

Thirdly, the capillary dispersivity function draws a contrast to this picture. Indeed, while the primary drainage leads to a continuous, bounded curve, the secondary and higher-order processes lead to capillary dispersivity curves that have a markedly different character. The curves diverge by more than an order of magnitude from the primary drainage reference curve, and jump discontinuously when the process changes from imbibition to drainage or vice versa. In the coarse model, the capillary dispersivity function also embodies gravitational forces, thus for gravitationally redistributive systems, we expect a pronounced effect of the higher-order drainage and imbibition processes. The redistribution is faster and the stationary state is reached quicker when hysteresis is taken into account (compare e.g. Figure 1a in [28]).

5. Conclusions

In this manuscript we have investigated the impact of a full hysteresis description, including both trapping and hysteresis of the bounding curves, in the fine-scale (3-dimensional) flow equations for CO_2 storage. We have considered this impact in terms of how the fine-scale hysteresis is reflected in upscaled (two-dimensional) constitutive functions.

Our research has emphasized the applicability of simplified coarse constitutive functions, interpreted as obtained through simplified fine-scale constitutive laws. Furthermore, we have explicitly considered the coarse-scale constitutive functions, e.g. relative permeability and capillary pressure, during primary drainage, secondary imbibition, as well as tertiary drainage and quaternary imbibition. This sequence is typical for CO_2 storage.

We find that during the primary and secondary processes, fine-scale trapping is the dominant contributor to hysteresis in the coarse models. Thus, simplified models that account for trapping are able to adequately capture the qualitative features at this stage.

However, for higher-order processes, the sole source of hysteresis on the coarse scale is the hysteresis in the capillary pressure saturation relationship.

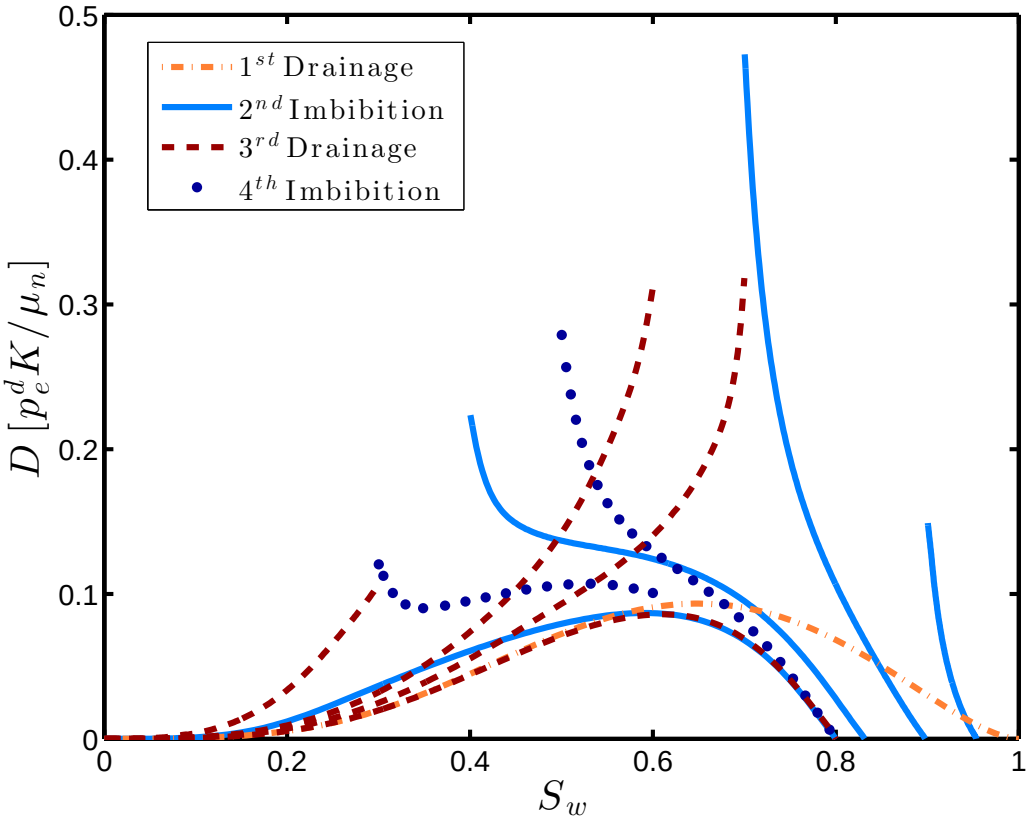

Figure 9: Capillary dispersivity functions for higher-order drainage and imbibition processes.

This is because for fine-scale trapping, i.e. Land's model, only the maximum non-wetting phase saturation $s_n^{\max}$ is of importance. The resulting impact on the coarse model can therefore only be addressed through the use of a full model for capillary trapping and hysteresis on the fine scale.

Beyond qualitative considerations, the quantitative impact can only be measured relative to specific case studies. To retain generality, we have therefore instead chosen to focus on the impact on the parameter functions that enter the typical fractional flow formulation. Here, we observe that there is only a minor impact of hysteresis on the fractional flow function, as the alterations in the relative permeability functions tend to cancel. In the fractional flow function for gravity driven plume migration the effects do not cancel each other but do not change the function drastically. The opposite conclusion holds for the capillary dispersivity function, wherein hysteresis

leads to peaks and discontinuities. Together, we interpret this in a general sense to imply that for advective processes, a correct fine-scale and upscaled treatment of hysteresis is of secondary importance, while for re-distributive processes hysteresis in the fine-scale constitutive functions plays an important role also at the coarse scale.

Acknowledgement

This work was supported in part by the National Science Foundation under Grant EAR-0934722; the Environmental protection Agency under Cooperative Agreement RD-83438501; and the Carbon Mitigation Initiative at Princeton University. It also forms part of the projects 215641, 199926 and 180679 of the Norwegian Science Foundation.

Appendix A.

In this appendix, we outline the numerical calculation of secondary-imbibition parameter-functions. These parameter functions require first the calculation of the primary drainage solution, since a secondary imbibition is a primary drainage followed by an imbibition. The fine-scale primary drainage saturation distribution s_w^{PD} for a given coarse-scale capillary pressure P_{cap}^{PD} is determined by

$$s_w^{PD}(z, P_{\text{cap}}^{PD}) = \begin{cases} s_{\text{cap}}^d \left[P_{\text{cap}}^{PD} - (\rho_w - \rho_n)gH(1-z)\right], \\ \qquad\qquad P_{\text{cap}}^{PD} > (\rho_w - \rho_n)gH(1-z), \\ 1, \qquad\qquad P_{\text{cap}}^{PD} \leq (\rho_w - \rho_n)gH(1-z). \end{cases} \tag{A.1}$$

We integrate that equation numerically to obtain a table of the inverse integrated capillary pressure-saturation relationship

$$S_w^{PD}(P_{\text{cap}}^{PD}) = \int_0^1 s_w^{PD}(z, P_{\text{cap}}^{PD})\mathrm{d}z. \tag{A.2}$$

The fine-scale saturation distribution of the secondary imbibition $s_w^{SI}(z, P_{\text{cap}}^{SI})$ is then obtained with the help of eq. (9) with

$$\bar{p}_{\text{cap}} = 0, \tag{A.3}$$
$$\bar{s}_w = 1, \tag{A.4}$$
$$\underline{\mathrm{p}}_{\text{cap}}(z) = P_{\text{cap}}^{PD} - (\rho_w - \rho_n)gH(1-z), \tag{A.5}$$
$$\underline{\mathrm{s}}_w = s_w^{PD}(z, P_{\text{cap}}^{PD}), \tag{A.6}$$
$$p_{\text{cap}} = P_{\text{cap}}^{SI} - (\rho_w - \rho_n)gH(1-z). \tag{A.7}$$

Note, however, that CO_2 gets trapped during imbibition and hence eq. (9) yields the apparent wetting-phase saturation σ_w^{SI} defined in eq. (13). To obtain the wetting phase saturation s_w^{SI}, we have to rearrange eq. (12) to express the disconnected non-wetting phase in terms of apparent wetting-phase saturation σ_w and $s_n^{\max}$. The maximum non-wetting phase saturation reached during the drainage obviously depends on z; it is obtained from the calculated primary drainage profile

$$s_n^{\max}(z, P_{\text{cap}}^{PD}) = 1 - s_w^{PD}(z, P_{\text{cap}}^{PD}). \tag{A.8}$$

Putting all together we can numerically calculate the fine-scale saturation distribution $s_w^{SI}(z, P_{\text{cap}}^{SI})$ and integrate it to obtain a coarse-scale capillary pressure-saturation relationship S_w^{SI}–P_{cap}^{SI} and relative permeabilities.

References

[2] Y. C. Yortsos, A theoretical analysis of vertical flow equilibrium, Transport in Porous Media 18 (1995) 107–129.

[1] B. Court, K. W. Bandilla, M. A. Celia, A. Janzen, M. Dobossy, J. M. Nordbotten, Applicability of vertical-equilibrium and sharp-interface assumptions in CO_2 sequestration modeling, International Journal of Greenhouse Gas Control 10 (2012) 134 – 147.

[3] M. Hesse, H. Tchelepi, B. Cantwell, F. Orr Jr., Gravity currents in horizontal porous layers: Transition from early to late self-similarity, J. Fluid Mech. 577 (2007) 363–383.

[4] R. Juanes, C. MacMinn, M. Szulczewski, The footprint of the CO_2 plume during carbon dioxide storage in saline aquifers: Storage efficiency

for capillary trapping at the basin scale, Transport In Porous Media 82 (2010) 19–30. 10.1007/S11242-009-9420-3.

[5] J. M. Nordbotten, M. A. Celia, An improved analytical solution for interface upconing around a well, Water Resources Research 42 (2006).

[6] J. M. Nordbotten, M. A. Celia, Similarity solutions for fluid injection into confined aquifers, Journal of Fluid Mechanics 561 (2006) 307–327.

[7] L. W. Lake, Enhanced Oil Recovery, Prentice Hall, New Jersey, 1989.

[8] J. Nordbotten, M. Celia, Geological Storage of CO_2: Modeling Approaches for Large-Scale Simulation, Wiley, 2012.

[9] H. E. Huppert, A. W. Woods, Gravity driven flows in porous layers, J. Fluid Mech. 292 (1995) 55 69.

[10] J. M. Nordbotten, H. K. Dahle, Impact of the capillary fringe in vertically integrated models for CO_2 storage, Water Resources Research 47 (2011).

[11] J. Nordbotten, H. Dahle, Impact of Capillary Forces on Large-Scale Migration of CO_2, in: 18th Conference on Computational Methods for Water Resources, Barcelona, Spain.

[12] M. Golding, J. Neufeld, M. Hesse, H. Huppert, Two-phase gravity currents in porous media, J. Fluid Mech. 678 (2011) 248–270.

[13] V. Joekar, S. M. Hassanizadeh, A. Leijnse, Insights into the relationships among capillary pressure, saturation, interfacial area and relative permeability using pore-scale network modeling, Transport in Porous Media 74 (2008) 201219.

[14] F. Doster, P. A. Zegeling, R. Hilfer, Numerical solutions of a generalized theory for macroscopic capillarity, Phys. Rev. E 81 (2010) 036307.

[15] S. Hassanizadeh, M. A. Celia, H. Dahle, Dynamic effect in the capillary pressure-saturation relationship and its impacts unsaturated flow, Vadose Zone Journal 1 (2002) 38–57.

[16] L. Cueto-Felgueroso, R. Juanes, Nonlocal interface dynamics and pattern formation in gravity-driven unsaturated flow through porous media, Physical Review Letters 101 (2008) 244504.

[17] M. van Genuchten, A closed-form equation for predicting the hydraulic conductivity of unsaturated soils, Soil Sci. Soc. Am. J 44 (1980) 892–898.

[18] R. H. Brooks, A. T. Corey, Hydraulic properties of porous media, in: Hydrol. Pap., volume 3, Colorado State University, Fort Collins, 1964.

[19] B. Bennion, S. Bachu, Relative permeability characteristics for supercritical co$_2$ displacing water in a variety of potential sequestration zones in the western canada sedimentary basin, SPE (2005) 95547.

[20] A. Papafotiou, H. Sheta, R. Helmig, Numerical modeling of two-phase hysteresis combined with an interface condition for heterogeneous porous media, Computational Geosciences 14 (2010) 273–287.

[21] J. C. Parker, R. J. Lenhard, T. Kuppusamy, A parametric model for constitutive properties governing multiphase flow in porous media, Water Resources Research 23 (1987) 618–624.

[22] C. S. Land, Calculation of imbibition relative permeability for two- and three phase flow from rock properties, Trans. Am. Inst. Min. Metall. Pet. Eng. 243 (1968).

[23] S. E. Gasda, M. A. Celia, J. M. Nordbotten, Upslope plume migration and implications for geological CO_2 sequestration in deep, saline aquifers, The IES Journal Part A: Civil & Structural Engineering 1 (2008) 2–16.

[24] S. E. Gasda, J. M. Nordbotten, M. A. Celia, Vertical equilibrium with sub-scale analytical methods for geological CO_2 sequestration, Computational Geosciences 13 (2009) 469–481.

[25] K. Pruess, J. M. Nordbotten, K. Zhang, Numerical simulation studies of the long-term evolution of a CO_2 plume under a sloping caprock, paper presented at the TOUGH Symposium 2009, Lawrence Berkeley Natl. Lab., Berkeley, Calif., 14 16 Sept. (2009).

[26] F. Doster, J. Nordbotten, M. Celia, Hysteretic upscaled constitutive relationships for vertically integrated porous media flow, Computation and Visualization in Science (accepted 2012).

[27] J. M. Nordbotten, M. A. Celia, Analysis of plume extent using analytical solutions for co2 storage, in: 16th Conference on Computational Methods in Water Resources, 2006.

[28] M. Hesse, F. J. Orr, H. Tchelepi, Gravity currents with residual trapping, J. Fluid. Mech. 611 (2008) 35–60.

[29] B. Zhao, C. MacMinn, Syulczewski, J. Neufeld, H. H.E., R. Juanes, Interface pinning of immiscible gravity-exchange flows in porous media, Phys. Rev. E 87 (2013) 023015.

[30] S. Gasda, J. M. Nordbotten, M. Celia, Vertically averaged approaches for CO_2 migration with solubility trapping, Water Resour. Res 47 (2011) W05528.

[31] K. Aziz, A. Settari, Petroleum reservoir simulation, Applied Science Publishers LTD, London, 1979.

[32] C. W. MacMinn, M. L. Szulczewski, R. Juanes, CO_2 Migration In Saline Aquifers. Part 1. Capillary Trapping Under Slope And Groundwater Flow, Journal Of Fluid Mechanics 662 (2010) 329–351.

References

[1] B. Court, K. W. Bandilla, M. A. Celia, A. Janzen, M. Dobossy, J. M. Nordbotten, Applicability of vertical-equilibrium and sharp-interface assumptions in CO_2 sequestration modeling, International Journal of Greenhouse Gas Control 10 (2012) 134 – 147.

[2] Y. C. Yortsos, A theoretical analysis of vertical flow equilibrium, Transport in Porous Media 18 (1995) 107–129.

[3] M. Hesse, H. Tchelepi, B. Cantwell, F. Orr Jr., Gravity currents in horizontal porous layers: Transition from early to late self-similarity, J. Fluid Mech. 577 (2007) 363–383.

[4] R. Juanes, C. MacMinn, M. Szulczewski, The footprint of the CO_2 plume during carbon dioxide storage in saline aquifers: Storage efficiency for capillary trapping at the basin scale, Transport In Porous Media 82 (2010) 19–30. 10.1007/S11242-009-9420-3.

[5] J. M. Nordbotten, M. A. Celia, An improved analytical solution for interface upconing around a well, Water Resources Research 42 (2006).

[6] J. M. Nordbotten, M. A. Celia, Similarity solutions for fluid injection into confined aquifers, Journal of Fluid Mechanics 561 (2006) 307–327.

[7] L. W. Lake, Enhanced Oil Recovery, Prentice Hall, New Jersey, 1989.

[8] J. Nordbotten, M. Celia, Geological Storage of CO_2, Wiley, 2012.

[9] H. E. Huppert, A. W. Woods, Gravity driven flows in porous layers, J. Fluid Mech. 292 (1995) 55 69.

[10] J. M. Nordbotten, H. K. Dahle, Impact of the capillary fringe in vertically integrated models for CO_2 storage, Water Resources Research 47 (2011).

[11] J. Nordbotten, H. Dahle, Impact of Capillary Forces on Large-Scale Migration of CO_2, in: 18th Conference on Computational Methods for Water Resources, Barcelona, Spain.

[12] M. Golding, J. Neufeld, M. Hesse, H. Huppert, Two-phase gravity currents in porous media, J. Fluid Mech. 678 (2011) 248–270.

[13] V. Joekar, S. M. Hassanizadeh, A. Leijnse, Insights into the relationships among capillary pressure, saturation, interfacial area and relative permeability using pore-scale network modeling, Transport in Porous Media 74 (2008) 201219.

[14] F. Doster, P. A. Zegeling, R. Hilfer, Numerical solutions of a generalized theory for macroscopic capillarity, Phys. Rev. E 81 (2010) 036307.

[15] S. Hassanizadeh, M. A. Celia, H. Dahle, Dynamic effect in the capillary pressure-saturation relationship and its impacts unsaturated flow, Vadose Zone Journal 1 (2002) 38–57.

[16] L. Cueto-Felgueroso, R. Juanes, Nonlocal interface dynamics and pattern formation in gravity-driven unsaturated flow through porous media, Physical Review Letters 101 (2008) 244504.

[17] M. van Genuchten, A closed-form equation for predicting the hydraulic conductivity of unsaturated soils, Soil Sci. Soc. Am. J 44 (1980) 892–898.

[18] R. H. Brooks, A. T. Corey, Hydraulic properties of porous media, in: Hydrol. Pap., volume 3, Colorado State University, Fort Collins, 1964.

[19] B. Bennion, S. Bachu, Relative permeability characteristics for supercritical co$_2$ displacing water in a variety of potential sequestration zones in the western canada sedimentary basin, SPE (2005) 95547.

[20] A. Papafotiou, H. Sheta, R. Helmig, Numerical modeling of two-phase hysteresis combined with an interface condition for heterogeneous porous media, Computational Geosciences 14 (2010) 273–287.

[21] J. C. Parker, R. J. Lenhard, T. Kuppusamy, A parametric model for constitutive properties governing multiphase flow in porous media, Water Resources Research 23 (1987) 618–624.

[22] C. S. Land, Calculation of imbibition relative permeability for two- and three phase flow from rock properties, Trans. Am. Inst. Min. Metall. Pet. Eng. 243 (1968).

[23] S. E. Gasda, M. A. Celia, J. M. Nordbotten, Upslope plume migration and implications for geological CO_2 sequestration in deep, saline aquifers, The IES Journal Part A: Civil & Structural Engineering 1 (2008) 2–16.

[24] S. E. Gasda, J. M. Nordbotten, M. A. Celia, Vertical equilibrium with sub-scale analytical methods for geological CO_2 sequestration, Computational Geosciences 13 (2009) 469–481.

[25] K. Pruess, J. M. Nordbotten, K. Zhang, Numerical simulation studies of the long-term evolution of a CO_2 plume under a sloping caprock, paper presented at the TOUGH Symposium 2009, Lawrence Berkeley Natl. Lab., Berkeley, Calif., 14 16 Sept. (2009).

[26] F. Doster, J. Nordbotten, M. Celia, Hysteretic upscaled constitutive relationships for vertically integrated porous media flow, Computation and Visualization in Science (accepted 2012).

[27] J. M. Nordbotten, M. A. Celia, Analysis of plume extent using analytical solutions for co2 storage, in: 16th Conference on Computational Methods in Water Resources, 2006.

[28] M. Hesse, F. J. Orr, H. Tchelepi, Gravity currents with residual trapping, J. Fluid. Mech. 611 (2008) 35–60.

[29] B. Zhao, C. MacMinn, Syulczewski, J. Neufeld, H. H.E., R. Juanes, Interface pinning of immiscible gravity-exchange flows in porous media, Phys. Rev. E 87 (2013) 023015.

[30] S. Gasda, J. M. Nordbotten, M. Celia, Vertically averaged approaches for CO_2 migration with solubility trapping, Water Resour. Res 47 (2011) W05528.

[31] K. Aziz, A. Settari, Petroleum reservoir simulation, Applied Science Publishers LTD, London, 1979.

[32] C. W. MacMinn, M. L. Szulczewski, R. Juanes, CO_2 Migration In Saline Aquifers. Part 1. Capillary Trapping Under Slope And Groundwater Flow, Journal Of Fluid Mechanics 662 (2010) 329–351.